Statefinder analysis of scale-dependent cosmology

Pedro D. Alvarez *1, Benjamin Koch †2,3, Cristobal Laporte ‡4, Felipe Canales \S^2 , and Ángel Rincón \P^5

¹Departamento de Física, Universidad de Antofagasta, Aptdo. 02800, Chile

²Instituto de Física, Pontificia Católica Universidad de Chile, Av. Vicuña Mackenna 4860, Santiago, Chile

³Institut für Theoretische Physik, Technische Universität Wien, Wiedner Hauptstrasse 8-10, A-1040 Vienna, Austria and Atominstitut, Stadionalle 2, A-1020 Vienna, Austria
 ⁴Institute for Mathematics, Astrophysics and Particle Physics (IMAPP), Radboud University, Heyendaalseweg 135, 6525 AJ Nijmegen, The Netherlands

⁵Sede Esmeralda, Universidad de Tarapacá. Avda. Luis Emilio Recabarren 2477, Iquique, Chile.

Received: date / Revised version: date

Abstract

We study the state finder parameters of a cosmological model based on scale-dependent gravity. The effective Einstein field equations come from an average effective action. From the dynamical system, we derive analytical expressions that improve the convergence of the numerical solutions. We determine the state finder parameters for moderate redshift and compare them with well-known alternatives to $\Lambda {\rm CDM}.$

Contents

1	Introduction	2
	1.1 Idea and structure of this paper	3
	*E-mail: pedro.alvarez@uantof.cl	
	†E-mail: benjamin.koch@tuwien.ac.at	
	[‡] E-mail: cristobal.laportemunoz@ru.nl	
	§E-mail: facanales@uc.cl	
	$\P_{ ext{E-mail: aerinconr@academicos.uta.cl}}$	

		e motivation behind statefinder diagnostic	3
3	nari	tefinder parameters in the scale-dependent cosmological sce- io	5
	3.1	Comparison with other models	8
	3.2	Case $g'_0 > 0$	12
	3.3	Case $g_0' < 0$	15
	3.4	Case $a_0' > 0$	16
4	Cor	nclusions and final remarks	16

1 Introduction

Many predictions of Einstein's General Relativity [1] (GR) have been confirmed over the last 100 years. The most prominent of these tests are the classical tests and solar system tests [2–4], direct detections of gravitational waves [5–9], from black hole (BH) and neutron star mergers, and the first image of a black hole [10–15].

Shortly after the discovery of this successful theory as best theoretical description of gravitational phenomena, the question arose, whether this theory could fit into the framework of quantum field theory (QFT). Many promising attempts in this direction have been made. However, the quest is still open. This is in part due to the complexity of the theoretical framework and in part due to the lack of testable predictions and conclusive observational evidence.

Effective field theories (EFT) have proven to be an ideal theoretical instrument that allows to derive quantitative and testable predictions. This is both true in QFT and GR. Prominent approaches in GR include perturbative quantum gravity [16] and the non-perturbative asymptotic safety paradigm (for reviews see [17] and [18, 19]). A common feature of these EFT approaches is that they all have effective actions with scale-dependent (SD) couplings. Thus, studying theories with SD is an efficient way of exploring the phenomenological consequences of quantum field theories. This is also true for quantum gravity, where a full predictive quantum description is not yet available, but still exploring SD effects can give valuable phenomenological insight. In this context, after the necessary scale setting, working with the SD gravitational couplings G(x)(Newtons' coupling) and $\Lambda(x)$ (cosmological coupling), in the Einstein-Hilbert truncation is particularly useful. In this truncation, one incorporates aspects of quantum gravity (through SD) while still keeping the field equations second order. These second-order field equations can be complemented by an additional energy condition in such a way that they form a closed system that maintains general covariance [20, 21].

With this and related frameworks it was possible to obtain numerous novel results for SD black holes [21–41], and effects of SD in cosmology [42–49]. In a recent work we have developed a framework to study observational aspects of

this approach in late-time cosmology by addressing the Hubble tension in terms of SD [50].

This pleasing progress with SD cosmology is to be seen in context of numerous other models that also give viable phenomenology of the late evolution of the Universe [51–58]. Naturally, it would be interesting to investigate the similarities and differences of the SD approach with each of these models. However, this would mean that one would have to compare observable by observable across all these models. This is an increasingly costly task since the number of necessary comparisons grows factorial with the number of models and observables. This is where model-independent parametrizations of the cosmological evolution can provide a helpful tool to simplify this task. In particular, the statefinder diagnostic gives a common ground for the comparison of multiple cosmological models [59–63].

Further, the statefinder diagnostic is useful for discriminating cosmological models. The reason is that even models with very similar expansion histories can have discrepancies at higher order, which are perceivable in the statefinder approach. Thus, as statefinder diagnostic accounts for high order correction in derivatives on the scale factor, the approach is well suited to discriminate between seemingly equivalent models.

1.1 Idea and structure of this paper

The main idea of the paper is the following. Firstly, we reformulate the SD approach to cosmology to be suitable for a large-scale numerical study. The next step is to perform numerical analysis and compare it with related models. Finally, we analyze the results of this study by using the statefinder formalism, comparing our results with another coming from well-known papers.

The paper is organized as follows: in section 2, we present a brief self-contained discussion of the statefinder diagnostic. Then, in section 3, we summarize the statefinder approach in scale-dependent gravity, including the corresponding differential equations describing SD cosmology, and derive helpful formulas that improve the convergence of numerical solutions. Also, we compute the statefinder parameters as functions of redshift and compare them to well-known alternative cosmological models. Finally, we summarize with the take-home message and final remarks in section 4.

2 The motivation behind statefinder diagnostic

A large variety of cosmological models can be used to derive the expansion history of the Universe. Since, in many cases, the underlying motivation for each model is quite diverse, it becomes useful to have a purely geometrical way of characterizing models. Let us consider a Taylor expansion of the scale factor (the only free function in the FRW metric),

$$a(t) = a(t_0) + \dot{a}(t_0)(t - t_0) + \frac{1}{2!}\ddot{a}(t_0)(t - t_0)^2 + \frac{1}{3!}\ddot{a}(t_0)(t - t_0)^3 + \cdots$$
 (1)

The first derivative is related to the most important observable in cosmology, the Hubble parameter H(z), and with the second derivative, we can construct a dimensionless cosmological function, the deceleration parameter,

$$q \equiv -\frac{\ddot{a}/a}{H^2} \,, \tag{2}$$

q < 0 describes an accelerating universe. The deceleration parameter can also be expressed in terms of derivatives of H,

$$q(z) = -1 + \frac{H'(z)}{H(z)}(1+z), \qquad (3)$$

and therefore, H(z) and g(z) are observable because they can be inferred by luminosity distance or other measurements. Within the context of the $\Lambda \mathrm{CDM}$ there is a large degeneracy in the deceleration parameter that tells us that measuring q_0 is not enough to discriminate Λ CDM models with different values of the parameters $(\Omega_m, \Omega_{\Lambda})$. Thus, as different models could coincide in both H(z) and q(z), further geometrical parameters, the statefinder parameters, were proposed [59,60]. The statefinder parameters, r and s, are defined as follows

$$r = \frac{\ddot{a}}{aH^3}, \tag{4}$$

$$r = \frac{\ddot{a}}{aH^3},$$

$$s = \frac{r-1}{3(q-\frac{1}{2})},$$
(5)

where the dot represent differentiation with respect to the cosmic time t, H = \dot{a}/a is the Hubble parameter, and $q = -\ddot{a}/(aH^2)$ is the decelerating parameter. By combining q(z) with r(z) or s(z) we have a diagnostic pair that is very good at discriminating cosmological models. For example, from the Friedmann equation, we can see that the parameter s is extremely sensitive to the total pressure

$$s = \frac{\rho + p}{p} \frac{\dot{p}}{\dot{\rho}}.$$
 (6)

Therefore $s \to \infty$ when $p \to 0$. As pointed out in [60], for Λ CDM this occurs for $z_* \sim 10$. Therefore the parameter s diagnoses the presence of dark energy even at higher redshifts when the contribution of dark energy to the total energy is small. Also, the definition of the statefinder parameter r is motivated by removing the dependence on dark energy.

Different trajectories of the q-r plane or the q-s plane correspond to different dark matter and dark energy models. Thus, studying this "phase space" helps to identify the main features of a given cosmological model without any reference to the microscopic degrees of freedom. Notice that the pair $\{q, r\}$ or $\{q,s\}$ provide a good way of establishing the "distance" between two cosmological models. Let us define "the classical limit" of the SD cosmological model as the case when $\dot{g}(t_0) = 0$ (this definition is justified below). Such a case corresponds to the pair $\{r, s\} \equiv \{1, 0\}$, i.e., it corresponds to a spatially flat ΛCDM Universe up to a possible renormalization of the absolute value of the Newton constant $(g(t_0))$ may or may not be equal to 1).

In order to contrast with observations, there are two main strategies in the literature. Firstly, for concrete models, q(z), r(z), and s(z) can be inferred from the best fit values of the parameters of the model that are implied from observations. Such analysis have been applied to several dark energy models [64–68], see also [69] and references therein. Secondly, there are also attempts to reconstruct the parameters as functions of redshift geometrically. Although this is a hard task, there has been recent progress in this direction [69–71]. This work will take advantage of this formalism to answer if the scale-dependent gravity of [50] may correspond to a dynamically equivalent cosmological model. In this paper, we provide an answer to this question: scale-dependent gravity is an independent model, as can be seen by looking at the state finder parameters derived below.

3 Statefinder parameters in the scale-dependent cosmological scenario

The system of differential equations that determines the cosmological background evolution is formed by three equations [50]

$$\frac{1}{H_0^2} \left(H^2 - H \frac{\dot{g}}{g} \right) = \Omega_\Lambda \lambda(t) + \frac{\Omega_r}{a^4} g + \frac{\Omega_m}{a^3} g \,, \tag{7}$$

$$\frac{1}{H_0^2} \left(2\dot{H} + 3H^2 - 2H\frac{\dot{g}}{g} + 2\frac{\dot{g}^2}{g^2} - \frac{\ddot{g}}{g} \right) = 3\Omega_{\Lambda}\lambda(t) - \frac{\Omega_r}{a^4}g, \tag{8}$$

$$\frac{\ddot{g}}{g} - H\frac{\dot{g}}{g} - 2\frac{\dot{g}^2}{g^2} = 0, \tag{9}$$

where

$$g(t) = \frac{G(t)}{G_0}, \quad \lambda(t) = \frac{\Lambda(t)}{\Lambda_0}.$$
 (10)

As in the Λ CDM model, the density parameters Ω_m , Ω_r , and Ω_{Λ} describe the contents of the Universe. The time dependence of the Λ coupling that is implied in the scale-dependent scenario results in time-dependent dark energy

$$\Omega_{\Lambda}\lambda(t) = \frac{\Lambda(t)}{3H_0^2}.$$
 (11)

We will explore the phase space of the dynamical system given by Eqs. (7-9). For this discussion, it is convenient to use the dimensionless functions (10) and

$$x = \frac{a(t)}{a_0} \,. \tag{12}$$

The scale-dependent cosmological equations take the form

$$\frac{x'(\tau)^2}{x(\tau)^2} - \frac{g'(\tau)x'(\tau)}{g(\tau)x(\tau)} = \Omega_m g(\tau)x(\tau)^{-3} + \Omega_r g(\tau)x(\tau)^{-4} + \Omega_\Lambda \lambda(\tau), \tag{13}$$

$$\frac{x'(\tau)^2}{x(\tau)^2} - 2\frac{g'(\tau)x'(\tau)}{g(\tau)x(\tau)} + 2\frac{g'(\tau)^2}{g(\tau)^2} + 2\frac{x''(\tau)}{x(\tau)} - \frac{g''(\tau)}{g(\tau)} = -\Omega_r g(\tau)x(\tau)^{-4} + 3\Omega_\Lambda \lambda(\tau),$$
(14)

$$\frac{g''(\tau)}{g(\tau)} - \frac{g'(\tau)x'(\tau)}{g(\tau)x(\tau)} - 2\frac{g'(\tau)^2}{g(\tau)^2} = 0.$$
 (15)

The evolution of this dynamical system can be determined by giving the initial conditions $x(\tau_0)$, $x'(\tau_0)$, $g(\tau_0)$ and $g'(\tau_0)$, where we denoted τ_0 as the present value of the evolution coordinate τ . This means an increase from one to four d.o.f. with respect to the Λ CDM case, where only $x'(\tau_0)$ is required to provide initial values. In the Λ CDM case, this degree of freedom is quite often traded for the value of h.

When switching between the time variables t and τ is useful to have at hand the relations,

$$\dot{x}(t)/x(t) = (H_{100}h)x'(\tau)/x(\tau), \tag{16}$$

$$t = (H_{100}h)^{-1}\tau. (17)$$

In particular,

$$H_0 = (H_{100}h)x'(\tau_0)/x(\tau_0), \qquad (18)$$

$$t_{\text{age}} = (H_{100}h)^{-1}\tau_{\text{age}}.$$
 (19)

In [50], we found that the model (13)-(15) can release the tension on the Hubble constant inferred from the CMB and low redshift observations. A natural question arises: how to discriminate the dynamics derived from this model from the plethora of cosmological models available to date?

To answer this question, we will study the statefinder parameters of the scale-dependent scenario. We will focus on the effects of different values of the initial conditions while keeping the density parameters Ω_m , Ω_r , and Ω_{Λ} fixed. We will consider the fiducial values

$$\Omega_m = 0.7, \quad \Omega_r = 0, \quad \Omega_{\Lambda} = 1 - \Omega_m.$$
(20)

Exact solutions for the SD model are not known in general, and therefore we will consider numerical solutions,

$$(z, X) = (z(\tau), X(\tau)), \tag{21}$$

where X stands for a, H, q, r or s. Moreover, numerical stability becomes a problem in the evaluation of q, r and s and therefore it is convenient to obtain analytic expressions for H, q and r that lower the order in derivatives

of expressions that are evaluated numerically. We will do this by using the dynamical system (13)-(15). From the NEC, eq. (15) we get

$$\frac{g'}{g} = \frac{g_0'}{g_0} \frac{g}{g_0} \frac{x}{x_0} \,. \tag{22}$$

Also, substituting g'' from (15) and λ from (13) into (14) we get

$$\left(\frac{x'}{x}\right)' = f(x,g), \qquad (23)$$

where

$$f(x,g) = -2\Omega_r \frac{g}{x^4} - \frac{3}{2}\Omega_m \frac{g}{x^3}.$$
 (24)

The evaluation of the r.h.s. of equations (22), (23) has a much better numerical stability than the evaluation of the l.h.s. We will use this procedure to study H, q, r, and s for the SD model, and we will compare to the reference models Λ CDM, Brans-Dicke, quiessence, and kiessence.

For the Hubble parameter we have

$$H = hH_{100}\frac{x'}{x}\,, (25)$$

where

$$\frac{x'}{x} = \frac{x'_0}{x_0} + \int_{\tau_0}^{\tau} d\tilde{\tau} f(x(\tilde{\tau}), g(\tilde{\tau})). \tag{26}$$

Evaluation of the r.h.s. of (26) is more time consuming than evaluation of the l.h.s. but it offers better numerical stability. In the computation of H, numerical stability does not pose a serious problem in most cases, but for the computation of higher-order parameters, it is essential to use expressions with better numerical stability.

The parameters q, r, and s are dimensionless, meaning that their formal expressions in terms of time derivatives or derivatives with respect to τ remain the same,

$$q = -\frac{x''/x}{(x'/x)^2} \,, (27)$$

and so on for r and s. Using (23) we can rewrite q as

$$q = -1 - \frac{f(x,g)}{(x'/x)^2}, (28)$$

where in the denominator of the second term, we can either use the l.h.s. or the r.h.s. of (26), since in this case, the usage of l.h.s. of (26) does not introduce numerical instabilities in such term.

For r, which is defined by,

$$r = \frac{x'''/x}{(x'/x)^3},\tag{29}$$

we get

$$r = -q + \left(4\Omega_r \frac{g}{x^4} + \frac{3}{2}\Omega_m \frac{g}{x^3}\right) (x'/x)^{-2} + \left(\frac{g_0'}{g_0} \frac{g}{g_0} \frac{x}{x_0}\right) f(x,g).$$
 (30)

For numerical stability, it is sufficient to use (28) in the first term and the l.h.s. of (26) in the second term. Substituting q from (28) in (30) the r parameter can be written as

$$r = 1 + 2\Omega_r \frac{g}{x^4} (x'/x)^{-2} + \left(\frac{g_0'}{g_0} \frac{g}{g_0} \frac{x}{x_0}\right) f(x, g).$$
 (31)

From here, we see that r will remain pegged at 1 if $g'_0 = 0$ for the entire matter-dominated era, similar to what happens in Λ CDM. Compared to the Λ CDM we see that the term accompanying Ω_r gets an extra $g(\tau)$ factor,

$$r_{\Lambda CDM} = 1 + 2\Omega_r x^{-4} (H_0/H(t))^{-2}$$
. (32)

The parameter s can be evaluated by substituting (28) and (30) in (5).

Note that by using (22) in (23) we can obtain expressions free of derivatives of x and g for higher-order parameters. These techniques allowed us to evaluate the statefinder parameters for higher redshift without the need for Pade approximants, see for instance [72].

3.1 Comparison with other models

We will compare the SD model with referential models such as Λ CDM, quiessence, kinnesence, polynomial dark energy, and Brans-Dicke cosmological models. Before doing this, let us use (22) to answer a frequently asked question about the scale-dependent model: is the SD cosmological model equivalent to a Brans-Dicke theory? The answer is no. We can use (22) to obtain an integral expression for $q(\tau)$,

$$g = g_0 \left(1 - \frac{g_0'}{x_0 g_0} \int_{\tau_0}^{\tau} d\tilde{\tau} x(\tilde{\tau}) \right)^{-1}. \tag{33}$$

Therefore the dynamics of $g(\tau)$ predicted by the SD model is essentially different from the one predicted by the Brans-Dicke theory (BD), where

$$\frac{G}{G_0}\Big|_{\text{RD}} = x^{-\frac{1}{\omega+1}},$$
 (34)

and ω is a parameter present in the BD theory [73]. In the SD model, an initial condition $g'_0 = 0$ grants g = const for all t, but such behavior can only be obtained by an improper limit of the BD theory $\omega \to \infty$. There are, however, values of the initial conditions of the SD model that can reproduce almost exactly H(z) and the q(z) parameter in the BD theory and differences show up at higher order only, the behavior of the (see plots in Figures 3, 4 and 5 below).

We will also refer to other well-known cosmological models for comparison. We will include in our discussion the quiessence and kinessence models already discussed in [59,60]. Let us recall the equation of state

$$p = w\rho. (35)$$

In Λ CDM we have w=-1, in quiessence models we have w<-1/3 and in kinessence we have a time-dependent w or $w(z) \neq const$. A particular realization of kinessence is the quintessence model where an extra scalar field with a self-interaction potential minimally coupled to gravity [74,75]. In such models, the statefinder pair takes the form

$$r = 1 + \frac{9}{2}\Omega_X w(1+w) - \frac{3}{2}\Omega_X \frac{\dot{w}}{H},$$
 (36)

$$s = 1 + w - \frac{1}{3} \frac{\dot{w}}{wH} \,, \tag{37}$$

where the function w(t) can be related to a mixture of physical (Ω_X) and geometrical parameters (in this case q(t)),

$$w(t) = \frac{2q(t) - 1}{3\Omega_X}. (38)$$

We will also compare our results to a spatially flat dust-filled Universe in the Brans-Dicke theory [76], where the Hubble parameter is given by

$$H = \frac{H_0}{\sqrt{1 + \frac{5\omega + 6}{6(\omega + 1)^2}}} \sqrt{\Omega_m (1 + z)^{\frac{3\omega + 4}{\omega + 1}} + \Omega_\Lambda}.$$
 (39)

Constraints on the rate of variation of Newton constant, given in (34), provide that the parameter ω is constrained to $\omega > 40000$ [77,78]. Parameter estimation based on luminosity distances and the Union 2.1 compilation [79] gives the best fit parameters $\Omega_m = 0.296$ and $\Omega_{\Lambda} = 0.704$.

Finally, we will also compare to a polynomial dark energy model, where the dark energy density is expressed as a truncated Taylor series polynomial in (1+z) [80],

$$H(z) = H_0 \sqrt{\Omega_m (1+z)^3 + \rho_{DE}}, \quad \rho_{DE} = A_1 + A_2 (1+z) + A_3 (1+z)^2.$$
 (40)

The expression for the distance modulus is given by

$$\mu(z) = 5\log_{10} D_L(z) - 5\log_{10} H_0 + 52.38, \tag{41}$$

while luminosity distance reads,

$$\frac{D_L}{1+z} = \int_0^z \frac{dz}{\sqrt{\Omega_m (1+z)^3 + A_1 + A_2 (1+z) + A_3 (1+z)^2}}.$$
 (42)

We will use observational constraints coming from the following observations:

- The latest H(z) data, consisting in 28+1 data points given in [67]. Such dataset is based in 28 points given in [81] plus the value of H_0 estimated in [82].
- The Union 2.1 $\mu(z)$ data compilation consists of data for 833 SNe, drawn from 19 datasets. Of these, 580 SNe pass usability cuts [79].

These observations are sufficient to constrain reasonably well the following restricted versions of the polynomial DE model:

$$A_1 = 1 - \Omega_{\text{mat}}, A_2 = 0, \text{ 'model A'};$$
 (43)

$$A_3 = 1 - \Omega_{\text{mat}} - A_1, A_2 = 0, \text{ 'model B'}.$$
 (44)

We define χ^2 as

$$\chi^2 = \sum_{i=1}^n \left(\frac{y(z) - y_i^{\text{obs}}}{\sigma_i} \right)^2 , \qquad (45)$$

where y(z) represents model predictions for H(z) or $\mu(z)$. We determined the best fit parameters, and reduced chi-squared χ^2/ν , where ν is the number of degrees of freedom, $\nu(H(z)) = 26$ and $\nu(\mu(z)) = 577$ for both models, See table 1 with the results.

		H(z)	:)	$\mu(z)$		
		B.F.	M.V.	B.F.	M.V.	
		$\chi^2/\nu \approx 0.682$		$\chi^2/\nu \approx 0.974$		
'model	Ω_{mat}	0.261	$0.26^{+0.02}_{-0.02}$	0.281	$0.21^{+0.10}_{-0.12}$	
A,	H_0	80.118	$76.16^{+7.86}_{-8.92}$	70.350	$60.90^{+13.25}_{-9.53}$	
Α	A_3	-0.184	$-0.11^{+0.21}_{-0.13}$	-0.013	$0.31^{+0.52}_{-0.42}$	
		$\chi^2/\nu \approx 0.682$		$\chi^2/\nu \approx 0.974$		
ʻmodel	$\Omega_{ m mat}$	0.320	$0.32^{+0.06}_{-0.06}$	0.285	$0.31^{+0.20}_{-0.17}$	
B'	H_0	72.354	$72.11^{+2.04}_{-2.05}$	69.880	$69.92^{+0.43}_{-0.42}$	
Б	A_1	0.906	$0.90^{+0.13}_{-0.14}$	0.729	$0.75^{+0.18}_{-0.16}$	

Table 1: H_0 is given in units of [km s⁻¹Mpc⁻¹]. The reduced chi-squared values take the same value when rounded to the third decimal for both models.

We used the EMCEE Python library to implement the Markov chain Monte Carlo ensemble sampler that allows computation of maximum likelihood contours (M.L.C.) [83]. For 'model A', we obtain the results of figure 1, while for 'model B', the results are shown in figure 2. From the M.L.C. we can see that 'model B' gets better constrained by the H(z) and $\mu(z)$ data. Consequently, we will use the mean values within errors for 'model B' to provide us a reference region.

In figures 1c and 2c we have consider the mean values with 1σ error inferred from the $\mu(z)$ data (yellow shaded region), see last column of table 1. The gray shaded region correspond to models such that s(z) < 1 when z < 10, which is a

restriction that removes models that could alter the redshift value of the drag epoch.

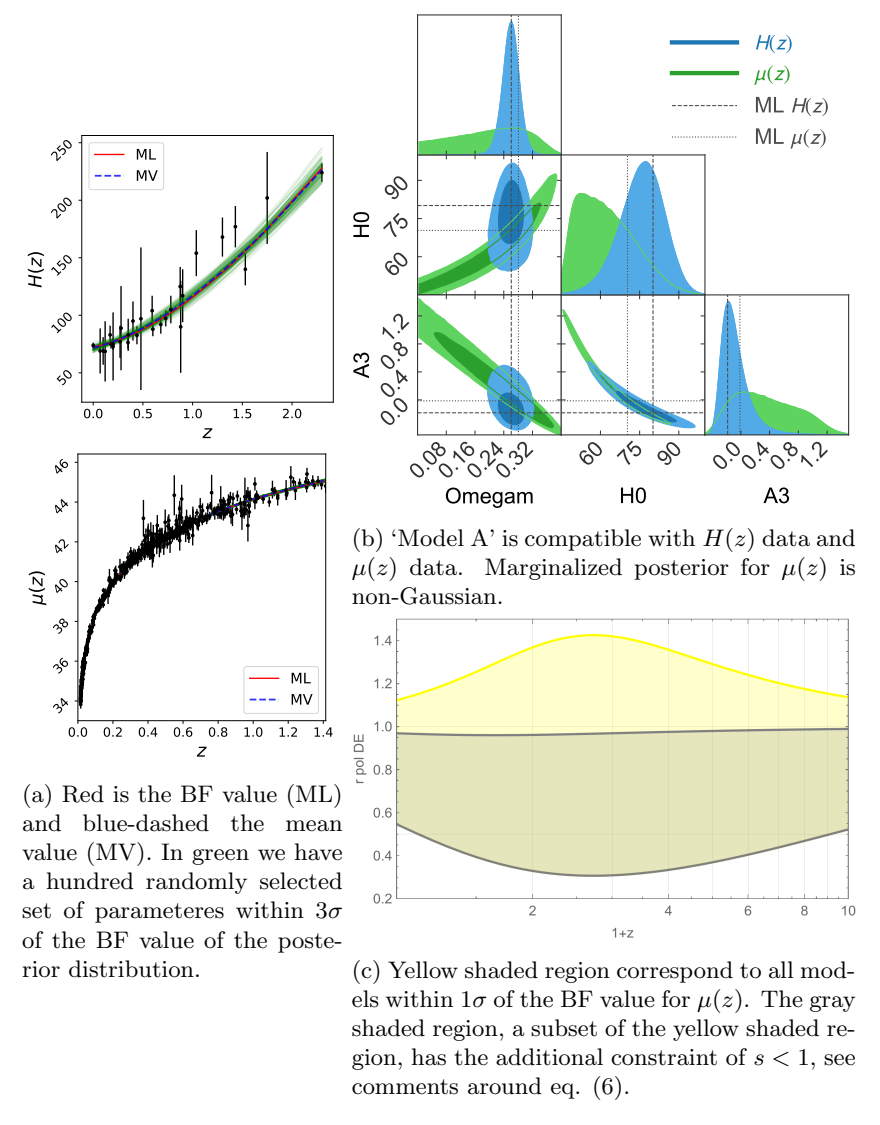


Figure 1: 'Model A' defined in eq. (43). Best fit values are summarized in table 1.

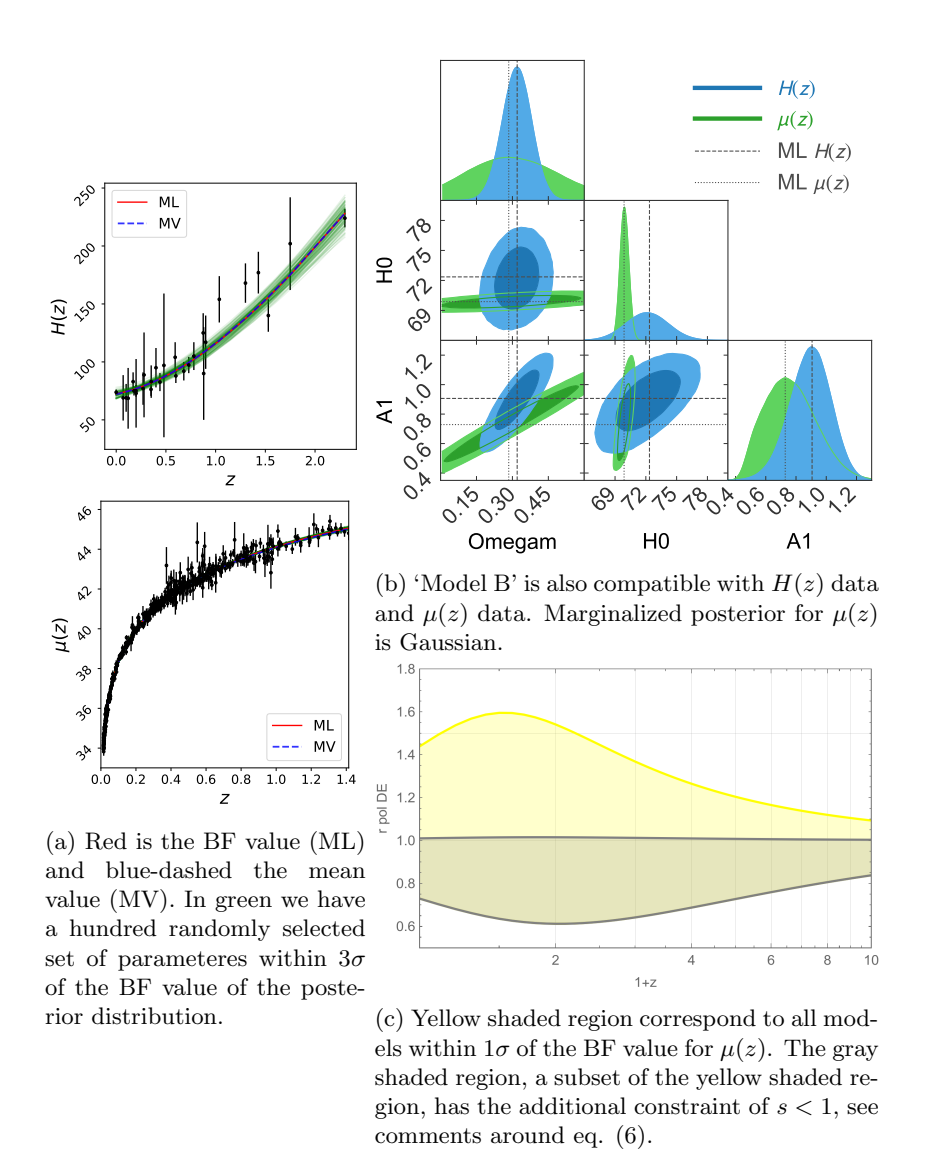


Figure 2: 'Model B' defined in eq. (44). Best fit values are summarized in table 1.

3.2 Case $g'_0 > 0$

In this section we will comment on the results for a given g'_0 positive and several values of x'_0 . We have considered $g'_0 = 1.0$ and $x'_0 = 0.40, 0.55, 0.70, 0.85, 1.00, 1.15$. Such models have curves for q, r, s that are easily distinguished in the plots of figure 3 and do not depend on h. The Hubble parameter, however, is not dimensionless and therefore also depends on the scale h of the time variable,

see (17). For this reason, the models displayed in the H(z) plot correspond to a value of h such that $t_{\rm age}$ determined from (19), give us roughly $t_{\rm age} \approx 13.8$ Gyrs See table 2.

The transition from deceleration to acceleration occurs at redshift z_t and the present deceleration value is q_0 , see right-most columns of table 2. When $g_0' \sim 0.1$, all the models with $x_0' \gtrsim 0.7$ exhibit acceleration/deceleration transition. The models with $x'_0 = 0.70, 0.85, 1.00, 1.15$ have $(z_t, q_0) = (0.10, -0.08)$, (0.44, -0.38), (0.71, -0.55), (0.94, -0.66) respectively. The transition for Λ CDM occurs at $z_t \approx 0.68$ (Planck values), or using the approximation $a = (\Omega_m/2\Omega_\Lambda)^{1/3}$, at $z_t \approx 0.66$ using Planck values [84]. This approximation uses the model that neglects Ω_{rad} so that we have the analytic solution

$$a(t) = (\Omega_m/\Omega_\Lambda) \sinh^{2/3}(t/t_\Lambda), \quad t_\Lambda = 2/(3H_0\sqrt{\Omega_\Lambda}),$$
 (46)

which is fairly accurate for a > 0.01 (or t > 10Myrs). The decceleration parameter is given by $q_0=1/2\Omega_m-\Omega_\Lambda$ in the $\Lambda {\rm CDM}$ model, and evaluates to $q_0 \approx -0.55$ for the Planck inferred parameters and $q_0 = -0.6 \pm 0.2$ for supernova constraints. For Brans-Dicke model it is obtained $q_0 \approx -0.56$. In [85], using combined constraints from H(z)+Union 2.1+NVSS-ISW (NRAO VLA Sky Survey and integrated Sachs-Wolfe effect) data the authors obtain $q_0 = -0.5808^{+0.17}_{-0.13}$ and $z_t = 0.724 \pm 0.047$ for Λ CDM model.

In [65], the authors considered a kink-like parametrization for q(z),

$$q(z) = q_f + \frac{q_i - q_f}{1 - (q_i/q_f) \left(\frac{1+z_t}{1+z}\right)^{1/\tau}}.$$
(47)

The dependence of r(z) deduced from the kink-like q(z) model ² is contained in the yellow regions of figures 1 and 2. In [65], the authors used observations from several supernovea datasets, BAO-CMB and CMB to obtain constraints on the parameters of the kink-like model. Their results using combined SALT2+BAO-CMB observations give $z_t = 0.64 \pm 0.025$ and $q_0 = -0.53^{+0.17}_{-0.13}$ (here we quoted the 1σ confidence intervals). For $x_0 \gtrsim 0.7$, our model with $y_0 = 0.1$ is compatible with a kink-like shaped q(z). Differences appear in the higher order parameters.

The r(z) parameter is harder to constrain. Values of $x'_0 \gtrsim 0.55$ are fully contained within the constrained parameters of 'Model B', see curves r(z) contained in bottom-left plot of figure 3. These curves are also compatible with constraints on parametric reconstructions [69] and non-parametric reconstructions [71,85] of the jerk parameter.

The s(z) parameter is depicted in bottom-right plot of figure 3. In the plot can be seen that models with $x'_0 \lesssim 0.7$ produce a divergent s for some z < 5. This is a reflection of particularity of the scale dependent cosmology (recall that we are considering models were $\Omega_{\rm rad} = 0$ exactly) and here the comments after (6) apply. Observables that are sensitive on s(z) can be used to constraint the

¹There are several other well-known parameterizations for the deceleration parameter, see [86] and references therein. ^2the statefinder r(z) is the same as the cosmographic jerk parameter j(z)

scale dependent cosmology. Models with $x_0 \gtrsim 0.7$ are reasonably safe within the constrained region of 'Model B'.

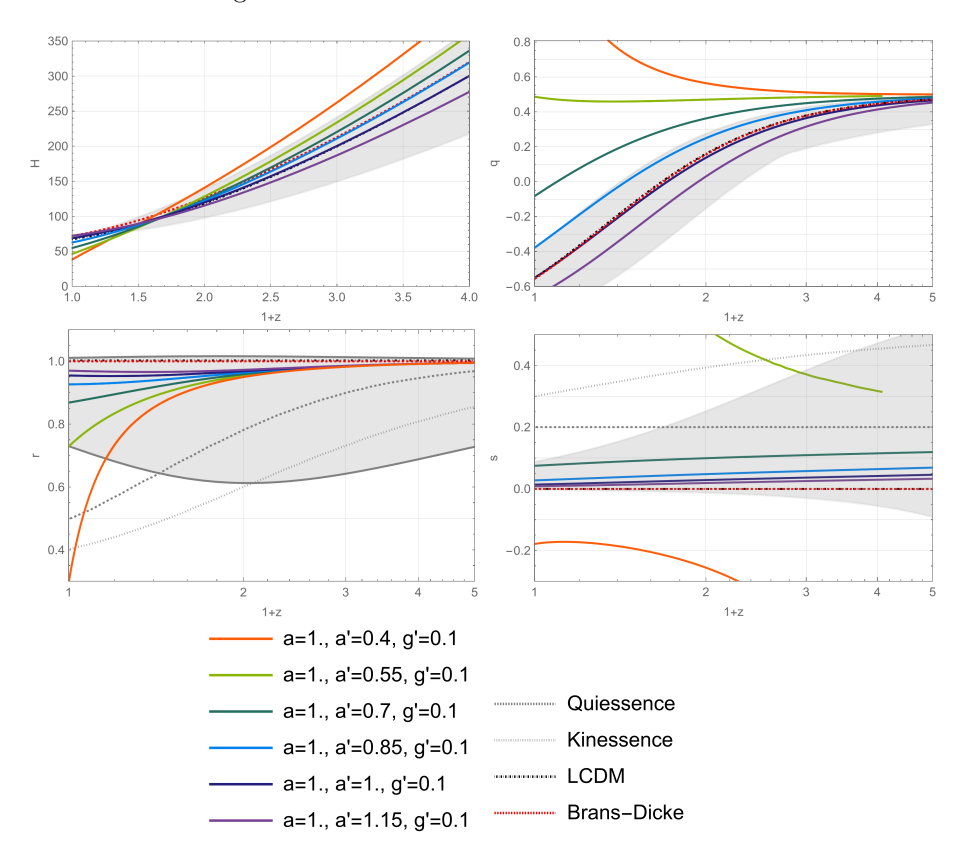


Figure 3: Comparison of the state finder parameters and H(z) for several models with fixed $g_0' > 0$. The plots are the following: top-left H(z), top-right q(z), bottom-left r(z) and bottom-right s(z). Colored lines correspond to different parameters of the scale dependent cosmology. Gray regions correspond to the allowed parameters in 'Model B' from H(z) and $\mu(z)$ observations. Dashed lines, stating other reference models, are indicated in the legend.

	x'_0	h	z_t	q_0
	0.40	0.96	_	1.81
$g_0 = 1.0$,	0.55	0.85	_	0.49
$x_0 = 1.0$,	0.70	0.79	0.10	-0.08
$g_0' = 0.1$	0.85	0.74	0.44	-0.38
90 0.1	1.00	0.69	0.71	-0.55
	1.15	0.63	0.94	-0.66

Table 2: Models with $g'_0 > 0$.

3.3 Case $g'_0 < 0$

In this section we will comment on the results for a given g'_0 negative and several values of x'_0 . For illustration purposes, we considered $g'_0 = -0.1$. Values of $x'_0 \sim 1$ get close to ΛCDM in H(z), q(z) and r(z), although z_t and q_0 get modified with respect to ΛCDM . From the bottom-left plot in figure 4, we can see that the model with negative g'_0 produces r > 1. From the bottom-right plot we can see that the parameter s exhibits large variations depending on the model. Therefore we can expect that constraints from $\mu(z)$ observations can impose strong restrictions on negative values of g'_0 if they are too high. As in the case $g'_0 > 0$, here we also see that z_t and q_0 depend on the value of x'_0 , see table 3.

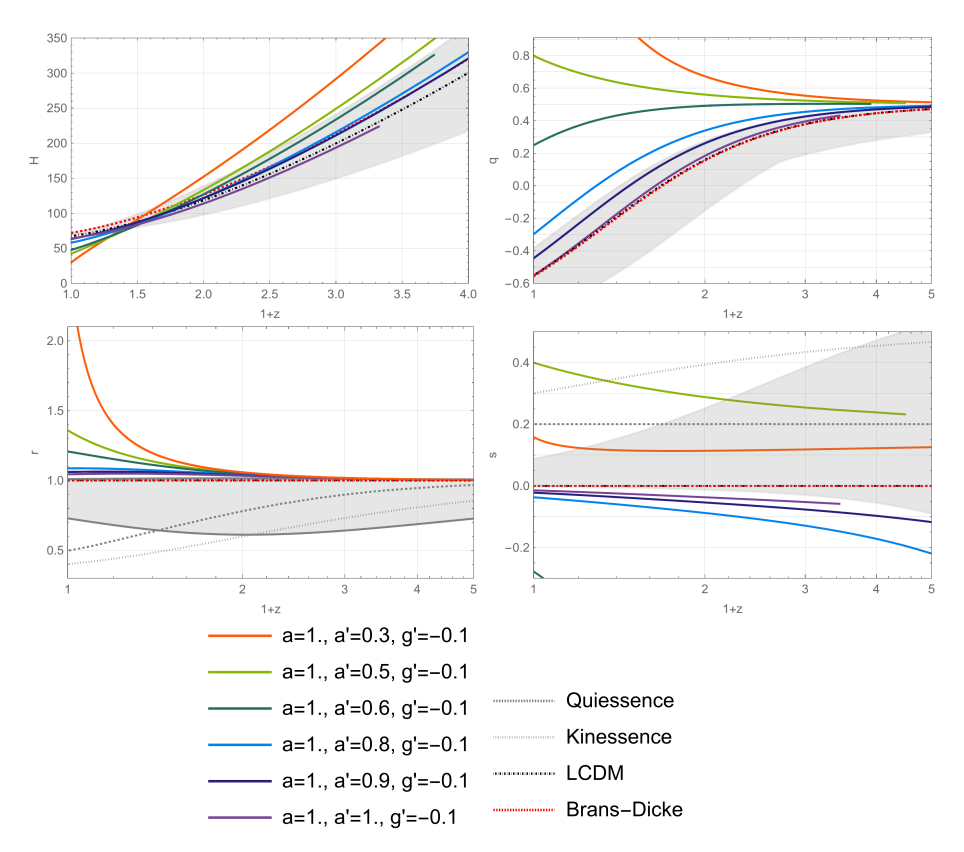


Figure 4: Comparison of the state finder parameters and H(z) for several models with fixed $g'_0 < 0$.

	x'_0	h	z_t	q_0
	0.3	1.00	_	4.00
$g_0 = 1.0,$ $x_0 = 1.0,$ $g'_0 = -0.1$	0.5	0.85	_	0.80
	0.6	0.80	_	0.25
	0.8	0.73	0.29	-0.30
	0.9	0.71	0.47	-0.44
	1.0	0.64	0.64	-0.55

Table 3: Models with $g_0' < 0$.

3.4 Case $a'_0 > 0$

In this section, we will comment on the results for a given a_0' positive and several values of g_0' . We have consider models where $g_0' \approx -0.5, -0.2, 0, 0.2, 0.5$. Plots of figure 5 make it clear that the scale-dependent model can get arbitrarily close to Λ CDM for $|g_0'|$ sufficiently small.

Plot q(z) of figure 5 shows that models where x_0' is chosen appropriately can be such that q_0 and $q_{z\to\infty}$ match the $\Lambda {\rm CDM}$ prediction. The redshift acceleration/deceleration transition gets modified, however, $z_t > z_t^{({\rm LCDM})}$ for $g_0' > 0$ and $z_t < z_t^{({\rm LCDM})}$ for $g_0' < 0$, see table 4.

Plots r(z) and s(z) of figure 5 can be used as an indication that $\mu(z)$ observations will prefer positive values of g'_0 .

	g_0'	h	z_t	q_0
	-0.5	0.63	0.51	-0.55
$g_0 = 1.0$,	-0.2	0.67	0.59	-0.55
$x_0 = 1.0$,	0	0.67	0.66	-0.55
$x_0' = 1.0$	0.2	0.67	0.76	-0.55
w ₀ 1.0	0.5	0.70	0.86	-0.55

Table 4: Models with $x'_0 = 1$.

4 Conclusions and final remarks

In this work, we reported statefinder parameters as functions of redshift for the scale-dependent cosmological model proposed in [50]. We provided analytical expressions that are helpful in finding numerical solutions. Our results provide a good guide for finding appropriate priors for the determination of maximum likelihood contours. Our study shows that for certain regions of the parameter space, the SD model predicts H(z) and q(z) very close to Brans-Dicke or Λ CDM models. Deviations can be seen at the level of r(z), but this parameter has weaker observational constraints.

The deceleration q(z) and jerk parameter r(z) allowed us to see an important property of the SD model: for generic initial conditions, the SD model has

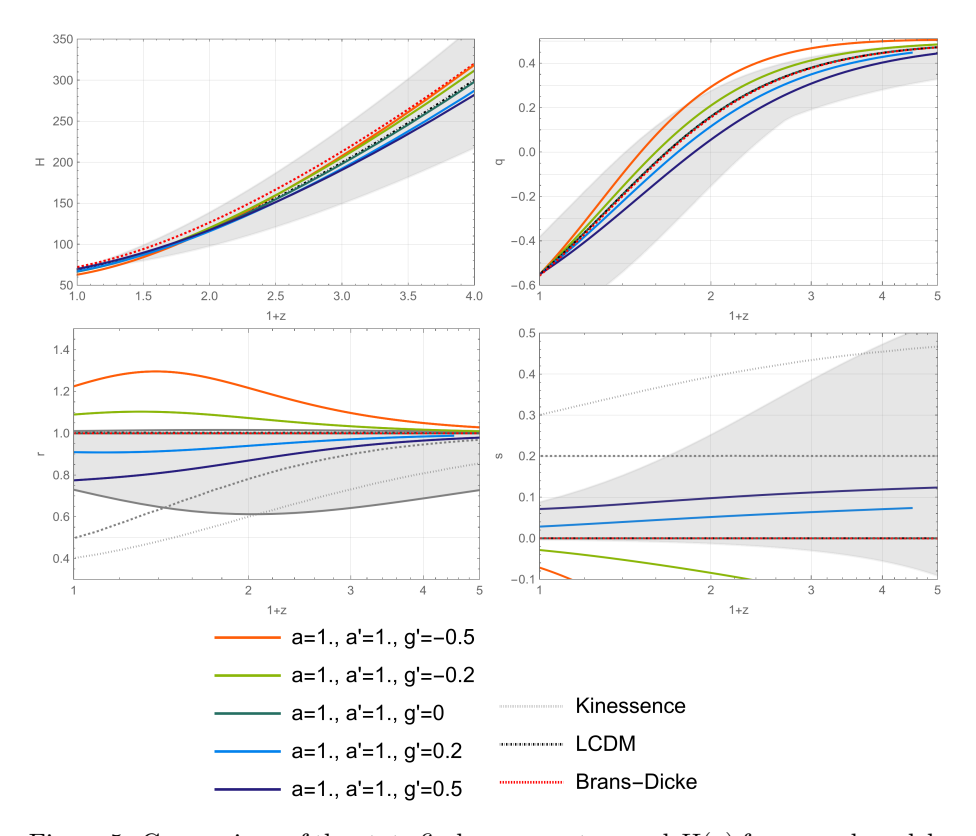


Figure 5: Comparison of the state finder parameters and H(z) for several models with fixed $x_0' = 1$.

convergence to the ΛCDM model for high redshift. Furthermore, the r-curves explored in figures 3 and 4 allowed us to see that upper and lower limits for $g_0'>0$ and $g_0'<0$ can be deduced from $\mu(z)$ observations. We propose such a study for a future work.

Our results for the jerk parameter r indicate (see e.g. bottom-left panels in figures 3 and 4) that there exist cases where r(z) will remain very close to Λ CDM for sufficiently big a_0' . Also, for the conditions given in figure 5, it can be seen that r(z) peaks at low redshifts $z \lesssim 1$, which is a particular behavior present in the SD model and is not observed in the other theories considered in this work.

The comparison with the allowed parameters in 'Model B' inferred from the distance modulus $\mu(z)$ observations in the statefinders diagnostic suggests the constraints $a' \gtrsim 0.6$ if $g'_0 \sim 0.1$ and $a' \gtrsim 0.9$ if $g'_0 \sim -0.1$. This set of constraints is thus helpful when defining realistic initial conditions of the SD scenario of gravity.

Additionally, we determine deceleration-acceleration transition z_t for several initial conditions. For models such that $q_0 \approx q_0(\text{LCDM}) \in (-0.55, -0.6)$, the

transition z_t is in the range $z_t \sim (0.7, 0.9)$ if $g_0' \sim 0.1$ or $z_t \sim (0.64, 0.7)$ if $g_0' \sim -0.1$. Smaller $|g_0'|$ values would give smaller deviations with respect to $z_t(\text{LCDM})$. It is interesting to note that the viscous fluid models also present a slightly earlier decelerated-accelerated transition compared with the one observed in the standard Λ CDM model, with values $z_t \approx 0.755$ [87]. Let us remark that the SD model does not include an early accelerated phase (besides the accelerated phase that begins at z_t) at higher redshifts such as the one at $z \sim 17.2$, as it has been observed in some Einstein-Gauss-Bonnet [88] and f(R) models [89]

The present study can be extended in various directions:

Observational constraints provided by H(z), $\mu(z)$ and BAO-CMB observations can be used to obtain maximum likelihood contours for the parameters of the SD model. The information provided in this paper is useful, and we are currently working on that topic for a separate publication.

SD scenario from a variational principle. The present model uses a NEC to close the system in (7)-(9). From a theoretical point of view, it would be interesting to explore the explicit form the possible actions that give to these equations. Attempts to derive this condition from an action require a non-trivial constraint on the Einstein-frame Ricci tensor from worldsheet string theory, see for instance, [90]. If we want to extend the current approach to field theories that do not satisfy some well-known energy conditions (including the NEC), we must look for an alternative route to close the system. One possible pathway relies upon fixing the renormalization scale in terms of the field variables by a variational procedure and then putting the scale on-shell [20, 43, 91]. Inputs for the beta functions of the couplings coming from quantum gravity could allow generating an extra gap equation, changing the dynamics of the SD scenario of cosmology. The inclusion of these quantum effects will be left for future work.

SD Brans-Dicke and K-essence and their relation with positivity bounds. By promoting the couplings in the BD and K-essence approaches to scale-dependent quantities, one can derive cosmological models that realize Weinberg's asymptotic safety scenario, see for instance [92,93]. It is interesting to study cosmological constraints of the effective parameters in those models in a reverse version of the positivity bounds program [94–96]. The latter uses unitarity, causality, and locality of effective field theories (EFT) to derive bounds on the EFT parameters that translate into stronger constraints parameters of the model [97].

Acknowlegements

C.L. acknowledges the scholarship Becas Chile, ANID-PCHA/2020-72210073 for financial support. The author A. R. acknowledges Universidad de Tarapacá for financial support.

References

- [1] Albert Einstein. The Foundation of the General Theory of Relativity. *Annalen Phys.*, 49(7):769–822, 1916.
- [2] Slava G. Turyshev. Experimental Tests of General Relativity. *Ann. Rev. Nucl. Part. Sci.*, 58:207–248, 2008.
- [3] Clifford M. Will. The Confrontation between General Relativity and Experiment. *Living Rev. Rel.*, 17:4, 2014.
- [4] Estelle Asmodelle. Tests of General Relativity: A Review. Bachelor thesis, Central Lancashire U., 2017.
- [5] B. P. Abbott et al. Observation of Gravitational Waves from a Binary Black Hole Merger. *Phys. Rev. Lett.*, 116(6):061102, 2016.
- [6] B. P. Abbott et al. GW151226: Observation of Gravitational Waves from a 22-Solar-Mass Binary Black Hole Coalescence. *Phys. Rev. Lett.*, 116(24):241103, 2016.
- [7] Benjamin P. Abbott et al. GW170104: Observation of a 50-Solar-Mass Binary Black Hole Coalescence at Redshift 0.2. Phys. Rev. Lett., 118(22):221101, 2017. [Erratum: Phys. Rev. Lett.121,no.12,129901(2018)].
- [8] B. P. Abbott et al. GW170814: A Three-Detector Observation of Gravitational Waves from a Binary Black Hole Coalescence. *Phys. Rev. Lett.*, 119(14):141101, 2017.
- [9] B.. P.. Abbott et al. GW170608: Observation of a 19-solar-mass Binary Black Hole Coalescence. *Astrophys. J.*, 851(2):L35, 2017.
- [10] Kazunori Akiyama et al. First M87 Event Horizon Telescope Results. I. The Shadow of the Supermassive Black Hole. Astrophys. J., 875(1):L1, 2019.
- [11] Kazunori Akiyama et al. First M87 Event Horizon Telescope Results. II. Array and Instrumentation. *Astrophys. J.*, 875(1):L2, 2019.
- [12] Kazunori Akiyama et al. First M87 Event Horizon Telescope Results. III. Data Processing and Calibration. *Astrophys. J.*, 875(1):L3, 2019.
- [13] Kazunori Akiyama et al. First M87 Event Horizon Telescope Results. IV. Imaging the Central Supermassive Black Hole. Astrophys. J., 875(1):L4, 2019.
- [14] Kazunori Akiyama et al. First M87 Event Horizon Telescope Results. V. Physical Origin of the Asymmetric Ring. *Astrophys. J.*, 875(1):L5, 2019.
- [15] Kazunori Akiyama et al. First M87 Event Horizon Telescope Results. VI. The Shadow and Mass of the Central Black Hole. Astrophys. J., 875(1):L6, 2019.

- [16] John F. Donoghue. General relativity as an effective field theory: The leading quantum corrections. *Phys. Rev. D*, 50:3874–3888, 1994.
- [17] Zvi Bern. Perturbative quantum gravity and its relation to gauge theory. Living Rev. Rel., 5:5, 2002.
- [18] Max Niedermaier and Martin Reuter. The Asymptotic Safety Scenario in Quantum Gravity. *Living Rev. Rel.*, 9:5–173, 2006.
- [19] Astrid Eichhorn. An asymptotically safe guide to quantum gravity and matter. Front. Astron. Space Sci., 5:47, 2019.
- [20] Benjamin Koch, Paola Rioseco, and Carlos Contreras. Scale Setting for Self-consistent Backgrounds. *Phys. Rev. D*, 91(2):025009, 2015.
- [21] Ángel Rincón and Benjamin Koch. On the null energy condition in scale dependent frameworks with spherical symmetry. *J. Phys. Conf. Ser.*, 1043(1):012015, 2018.
- [22] Carlos Contreras, Benjamin Koch, and Paola Rioseco. Black hole solution for scale-dependent gravitational couplings and the corresponding coupling flow. *Class. Quant. Grav.*, 30:175009, 2013.
- [23] Benjamin Koch and Frank Saueressig. Black holes within Asymptotic Safety. Int. J. Mod. Phys. A, 29(8):1430011, 2014.
- [24] Benjamin Koch and Paola Rioseco. Black Hole Solutions for Scale Dependent Couplings: The de Sitter and the Reissner-Nordström Case. *Class. Quant. Grav.*, 33:035002, 2016.
- [25] Benjamin Koch, Ignacio A. Reyes, and Ángel Rincón. A scale dependent black hole in three-dimensional space—time. *Class. Quant. Grav.*, 33(22):225010, 2016.
- [26] Ángel Rincón, Benjamin Koch, and Ignacio Reyes. BTZ black hole assuming running couplings. *J. Phys. Conf. Ser.*, 831(1):012007, 2017.
- [27] Ángel Rincón, Ernesto Contreras, Pedro Bargueño, Benjamin Koch, Grigorios Panotopoulos, and Alejandro Hernández-Arboleda. Scale dependent three-dimensional charged black holes in linear and non-linear electrodynamics. Eur. Phys. J., C77(7):494, 2017.
- [28] Ernesto Contreras, Ángel Rincón, Benjamin Koch, and Pedro Bargueño. A regular scale-dependent black hole solution. Int. J. Mod. Phys., D27(03):1850032, 2017.
- [29] Ernesto Contreras, Ángel Rincón, Benjamin Koch, and Pedro Bargueño. Scale-dependent polytropic black hole. Eur. Phys. J., C78(3):246, 2018.

- [30] E. Contreras and P. Bargueño. Scale—dependent Hayward black hole and the generalized uncertainty principle. *Mod. Phys. Lett.*, A33(32):1850184, 2018.
- [31] Ernesto Contreras, Ángel Rincón, and J. M. Ramírez-Velasquez. Relativistic dust accretion onto a scale–dependent polytropic black hole. *Eur. Phys. J.*, C79(1):53, 2019.
- [32] Ángel Rincón and Benjamin Koch. Scale-dependent rotating BTZ black hole. Eur. Phys. J., C78(12):1022, 2018.
- [33] Ángel Rincón, Ernesto Contreras, Pedro Bargueño, Benjamin Koch, and Grigorios Panotopoulos. Scale-dependent (2+1)-dimensional electrically charged black holes in Einstein-power-Maxwell theory. Eur. Phys. J., C78(8):641, 2018.
- [34] Ernesto Contreras and Pedro Bargueño. A self-sustained traversable scale-dependent wormhole. *Int. J. Mod. Phys.*, D27(09):1850101, 2018.
- [35] Ángel Rincón and Grigoris Panotopoulos. Quasinormal modes of scale dependent black holes in (1+2)-dimensional Einstein-power-Maxwell theory. *Phys. Rev.*, D97(2):024027, 2018.
- [36] Ángel Rincón, Ernesto Contreras, Pedro Bargueño, and Benjamin Koch. Scale-dependent planar Anti-de Sitter black hole. Eur. Phys. J. Plus, 134(11):557, 2019.
- [37] Ernesto Contreras, Ángel Rincón, Grigoris Panotopoulos, Pedro Bargueño, and Benjamin Koch. Black hole shadow of a rotating scale—dependent black hole. 2019.
- [38] E. Contreras, Á. Rincón, and P. Bargueño. Five-Dimensional Scale-Dependent Black Holes with Constant Curvature and Solv Horizons. Eur. Phys. J. C, 80(5):367, 2020.
- [39] P. Bargueño, J. A. Miralles, and J. A. Pons. Thermodynamics of spherically symmetric black holes in scale-dependent gravity. *Eur. Phys. J. C*, 80(12):1156, 2020.
- [40] Ángel Rincón, Ernesto Contreras, Pedro Bargueño, Benjamin Koch, and Grigoris Panotopoulos. Four dimensional Einstein-power-Maxwell black hole solutions in scale-dependent gravity. *Phys. Dark Univ.*, 31:100783, 2021.
- [41] Johanna N. Borissova, Aaron Held, and Niayesh Afshordi. Scale-Invariance at the Core of Quantum Black Holes. 3 2022.
- [42] A. Bonanno and M. Reuter. Cosmology of the Planck era from a renormalization group for quantum gravity. *Phys. Rev.*, D65:043508, 2002.

- [43] Benjamin Koch and Israel Ramirez. Exact renormalization group with optimal scale and its application to cosmology. *Class. Quant. Grav.*, 28:055008, 2011.
- [44] Ippocratis D. Saltas. Higgs inflation and quantum gravity: An exact renormalisation group approach. *JCAP*, 02:048, 2016.
- [45] Felipe Canales, Benjamin Koch, Cristobal Laporte, and Angel Rincon. Cosmological constant problem: deflation during inflation. 2018.
- [46] Nicolas R. Bertini, Wiliam S. Hipólito-Ricaldi, Felipe de Melo-Santos, and Davi C. Rodrigues. Cosmological framework for renormalization group extended gravity at the action level. Eur. Phys. J. C, 80(5):479, 2020. [Erratum: Eur.Phys.J.C 80, 644 (2020)].
- [47] Alessia Platania. The inflationary mechanism in Asymptotically Safe Gravity. *Universe*, 5(8):189, 2019.
- [48] Pedro Bargueño, Ernesto Contreras, and Ángel Rincón. Thermodynamics of scale-dependent Friedmann equations. Eur. Phys. J. C, 81(5):477, 2021.
- [49] Alessia Platania. From renormalization group flows to cosmology. Front. in Phys., 8:188, 2020.
- [50] Pedro D. Alvarez, Benjamin Koch, Cristobal Laporte, and Ángel Rincón. Can scale-dependent cosmology alleviate the H_0 tension? JCAP, 06:019, 2021
- [51] Joan Sola Peracaula. The Cosmological Constant Problem and Running Vacuum in the Expanding Universe. 3 2022.
- [52] Elcio Abdalla et al. Cosmology intertwined: A review of the particle physics, astrophysics, and cosmology associated with the cosmological tensions and anomalies. *JHEAp*, 34:49–211, 2022.
- [53] Cristian Moreno-Pulido and Joan Sola Peracaula. Renormalizing the vacuum energy in cosmological spacetime: implications for the cosmological constant problem. 1 2022.
- [54] C. P. Singh and Joan Sola Peracaula. Friedmann cosmology with decaying vacuum density in Brans–Dicke theory. Eur. Phys. J. C, 81(10):960, 2021.
- [55] Mehdi Rezaei, Joan Solà Peracaula, and Mohammad Malekjani. Cosmographic approach to Running Vacuum dark energy models: new constraints using BAOs and Hubble diagrams at higher redshifts. *Mon. Not. Roy. Astron. Soc.*, 509(2):2593–2608, 2021.
- [56] Joan Solà Peracaula, Adrià Gómez-Valent, Javier de Cruz Perez, and Cristian Moreno-Pulido. Running vacuum against the H_0 and σ_8 tensions. EPL, 134(1):19001, 2021.

- [57] Grigoris Panotopoulos, Ángel Rincón, Giovanni Otalora, and Nelson Videla. Dynamical systems methods and statender diagnostic of interacting vacuum energy models. *Eur. Phys. J. C*, 80(3):286, 2020.
- [58] Grigoris Panotopoulos and Ángel Rincón. Growth index and statefinder diagnostic of Oscillating Dark Energy. *Phys. Rev. D*, 97(10):103509, 2018.
- [59] Varun Sahni, Tarun Deep Saini, Alexei A. Starobinsky, and Ujjaini Alam. Statefinder: A New geometrical diagnostic of dark energy. *JETP Lett.*, 77:201–206, 2003.
- [60] Ujjaini Alam, Varun Sahni, Tarun Deep Saini, and A. A. Starobinsky. Exploring the expanding universe and dark energy using the Statefinder diagnostic. Mon. Not. Roy. Astron. Soc., 344:1057, 2003.
- [61] Xin Zhang. Statefinder diagnostic for holographic dark energy model. Int. J. Mod. Phys. D, 14:1597–1606, 2005.
- [62] A. K. D. Evans, I. K. Wehus, O. Gron, and Oystein Elgaroy. Geometrical constraints on dark energy. Astron. Astrophys., 430:399–410, 2005.
- [63] Jun Li, Rongjia Yang, and Bohai Chen. Discriminating dark energy models by using the statefinder hierarchy and the growth rate of matter perturbations. JCAP, 12:043, 2014.
- [64] Suresh Kumar. Observational constraints on Hubble constant and deceleration parameter in power-law cosmology. Mon. Not. Roy. Astron. Soc., 422:2532–2538, 2012.
- [65] R. Giostri, M. Vargas dos Santos, I. Waga, R. R. R. Reis, M. O. Calvão, and B. L. Lago. From cosmic deceleration to acceleration: new constraints from SN Ia and BAO/CMB. *JCAP*, 03:027, 2012.
- [66] Victor H. Cardenas, Carla Bernal, and Alexander Bonilla. Cosmic slowing down of acceleration using f_{gas} . Mon. Not. Roy. Astron. Soc., 433:3534, 2013.
- [67] Sarita Rani, A. Altaibayeva, M. Shahalam, J. K. Singh, and R. Myrzakulov. Constraints on cosmological parameters in power-law cosmology. *JCAP*, 03:031, 2015.
- [68] David Camarena and Valerio Marra. Local determination of the Hubble constant and the deceleration parameter. Phys. Rev. Res., 2(1):013028, 2020.
- [69] Abdulla Al Mamon and Kazuharu Bamba. Observational constraints on the jerk parameter with the data of the Hubble parameter. Eur. Phys. J. C, 78(10):862, 2018.

- [70] Zhong-Xu Zhai, Ming-Jian Zhang, Zhi-Song Zhang, Xian-Ming Liu, and Tong-Jie Zhang. Reconstruction and constraining of the jerk parameter from OHD and SNe Ia observations. *Phys. Lett. B*, 727:8–20, 2013.
- [71] Purba Mukherjee and Narayan Banerjee. Nonparametric reconstruction of interaction in the cosmic dark sector. *Phys. Rev. D*, 103(12):123530, 2021.
- [72] Salvatore Capozziello, Rocco D'Agostino, and Orlando Luongo. Rational approximations of f(R) cosmography through Padé polynomials. JCAP, 05:008, 2018.
- [73] Orest Hrycyna and Marek Szydlowski. Brans-Dicke theory and the emergence of ΛCDM model. *Phys. Rev. D*, 88(6):064018, 2013.
- [74] Varun Sahni and Alexei A. Starobinsky. The Case for a positive cosmological Lambda term. Int. J. Mod. Phys. D, 9:373–444, 2000.
- [75] Varun Sahni. The Cosmological constant problem and quintessence. Class. Quant. Grav., 19:3435–3448, 2002.
- [76] Gopi Kant Goswami. Cosmological parameters for spatially flat dust filled Universe in Brans-Dicke theory. Res. Astron. Astrophys., 17(3):27, 2017.
- [77] B. Bertotti, L. Iess, and P. Tortora. A test of general relativity using radio links with the Cassini spacecraft. *Nature*, 425:374–376, 2003.
- [78] Antonio De Felice, Gianpiero Mangano, Pasquale D. Serpico, and Mark Trodden. Relaxing nucleosynthesis constraints on brans-dicke theories. *Phys. Rev. D*, 74:103005, 2006.
- [79] N. Suzuki, D. Rubin, C. Lidman, G. Aldering, R. Amanullah, K. Barbary, L. F. Barrientos, J. Botyanszki, M. Brodwin, N. Connolly, K. S. Dawson, A. Dey, M. Doi, M. Donahue, S. Deustua, P. Eisenhardt, E. Ellingson, L. Faccioli, V. Fadeyev, H. K. Fakhouri, A. S. Fruchter, D. G. Gilbank, M. D. Gladders, G. Goldhaber, A. H. Gonzalez, A. Goobar, A. Gude, T. Hattori, H. Hoekstra, E. Hsiao, X. Huang, Y. Ihara, M. J. Jee, D. Johnston, N. Kashikawa, B. Koester, K. Konishi, M. Kowalski, E. V. Linder, L. Lubin, J. Melbourne, J. Meyers, T. Morokuma, F. Munshi, C. Mullis, T. Oda, N. Panagia, S. Perlmutter, M. Postman, T. Pritchard, J. Rhodes, P. Ripoche, P. Rosati, D. J. Schlegel, A. Spadafora, S. A. Stanford, V. Stanishev, D. Stern, M. Strovink, N. Takanashi, K. Tokita, M. Wagner, L. Wang, N. Yasuda, and H. K. C. Yee. Thehubble space telescopecluster supernova survey. v. improving the dark-energy constraints abovez; 1 and building an early-type-hosted supernova sample. The Astrophysical Journal, 746(1):85, Jan 2012.
- [80] Tarun Deep Saini, Somak Raychaudhury, Varun Sahni, and Alexei A. Starobinsky. Reconstructing the cosmic equation of state from supernova distances. *Phys. Rev. Lett.*, 85:1162–1165, 2000.

- [81] Omer Farooq and Bharat Ratra. Hubble parameter measurement constraints on the cosmological deceleration-acceleration transition redshift. Astrophys. J. Lett., 766:L7, 2013.
- [82] Adam G. Riess, Lucas Macri, Stefano Casertano, Hubert Lampeitl, Henry C. Ferguson, Alexei V. Filippenko, Saurabh W. Jha, Weidong Li, and Ryan Chornock. A 3% Solution: Determination of the Hubble Constant with the Hubble Space Telescope and Wide Field Camera 3. Astrophys. J., 730:119, 2011. [Erratum: Astrophys.J. 732, 129 (2011)].
- [83] Daniel Foreman-Mackey, David W. Hogg, Dustin Lang, and Jonathan Goodman. emcee: The MCMC Hammer. *Publ. Astron. Soc. Pac.*, 125:306–312, 2013.
- [84] N. Aghanim et al. Planck 2018 results. VI. Cosmological parameters. Astron. Astrophys., 641:A6, 2020. [Erratum: Astron. Astrophys. 652, C4 (2021)].
- [85] Syed Faisal ur Rahman. Constraining deceleration, jerk and transition redshift using cosmic chronometers, Type Ia supernovae and ISW effect. 8 2021.
- [86] Abdulla Al Mamon. Constraints on a generalized deceleration parameter from cosmic chronometers. *Mod. Phys. Lett. A*, 33(10n11):1850056, 2018.
- [87] L. Herrera-Zamorano, Miguel A. García-Aspeitia, and A. Hernández-Almada. Constraints and cosmography of ΛCDM in presence of viscosity. Eur. Phys. J. C, 80(7):637, 2020.
- [88] Miguel A. García-Aspeitia and A. Hernández-Almada. Einstein-Gauss-Bonnet gravity: Is it compatible with modern cosmology? *Phys. Dark Univ.*, 32:100799, 2021.
- [89] Luisa G. Jaime, Mariana Jaber, and Celia Escamilla-Rivera. New parametrized equation of state for dark energy surveys. *Phys. Rev. D*, 98(8):083530, 2018.
- [90] Maulik Parikh and Jan Pieter van der Schaar. Derivation of the Null Energy Condition. Phys. Rev. D, 91(8):084002, 2015.
- [91] Benjamin Koch and C. Laporte. Variational technique for gauge boson masses. *Phys. Rev. D*, 103(4):045011, 2021.
- [92] M. Reuter and H. Weyer. Renormalization group improved gravitational actions: A Brans-Dicke approach. *Phys. Rev.*, D69:104022, 2004.
- [93] C. Wetterich. Inflation, quintessence, and the origin of mass. Nucl. Phys. B, 897:111–178, 2015.

- [94] Allan Adams, Nima Arkani-Hamed, Sergei Dubovsky, Alberto Nicolis, and Riccardo Rattazzi. Causality, analyticity and an IR obstruction to UV completion. *JHEP*, 10:014, 2006.
- [95] Claudia de Rham, Scott Melville, Andrew J. Tolley, and Shuang-Yong Zhou. Positivity bounds for scalar field theories. *Phys. Rev. D*, 96(8):081702, 2017.
- [96] Claudia de Rham, Scott Melville, Andrew J. Tolley, and Shuang-Yong Zhou. UV complete me: Positivity Bounds for Particles with Spin. *JHEP*, 03:011, 2018.
- [97] Scott Melville and Johannes Noller. Positivity in the Sky: Constraining dark energy and modified gravity from the UV. *Phys. Rev. D*, 101(2):021502, 2020. [Erratum: Phys.Rev.D 102, 049902 (2020)].